

DBMC-aNOMAly: Asynchronous NOMA with Pilot-Symbol Optimization Protocol for Diffusion-Based Molecular Communication Networks

Alexander Wietfeld, *Graduate Student Member, IEEE*, Wolfgang Kellerer, *Fellow, IEEE*

arXiv:2512.07317v1 [cs.ET] 8 Dec 2025

Abstract—Multiple access (MA) schemes can enable cooperation between multiple nodes in future diffusion-based molecular communication (DBMC) networks. Non-orthogonal MA for DBMC networks (DBMC-NOMA) is a promising option for efficient simultaneous MA using a single molecule type. Expanding significantly upon previous work on the topic, this paper addresses the question of parameter optimization and bit error probability (BEP) reduction in an asynchronous network using DBMC-NOMA. First, we analytically derive the associated BEP and use the result for a thorough comparison with other MA schemes like time-division and molecule-division MA. We show that the asynchronous nature of the system can be exploited for performance gain, and the upper-bound performance can be achieved in all circumstances by avoiding a few worst-case offset configurations. Subsequently, we propose DBMC-aNOMAly, a pilot-symbol-based optimization protocol for asynchronous DBMC-NOMA, and extensively evaluate it using Monte-Carlo simulations. DBMC-aNOMAly is shown to provide robust BEP reduction for different network sizes, noise levels, subjected to sampling jitter, as well as for changing conditions during runtime, particularly, compared to protocols in previous work. DBMC-aNOMAly consists of a set of simple operations such as comparisons and additions, deliberately designed to be implementable with chemical reaction networks, setting up future work on the realistic modeling of the protocol.

Index Terms—Molecular communication, asynchronous, non-orthogonal multiple access, optimization algorithm, protocol

I. INTRODUCTION

MOLECULAR communication (MC) is a novel paradigm based on the transfer of information using molecules. Specifically, diffusion-based molecular communication (DBMC) is envisioned to play a major role as an energy-efficient and biocompatible approach at micro or nano-scales [3].

One of the main visions driving research into DBMC is the Internet of Bio-Nano-Things (IoBNT) [4], an interconnected network of tiny Bio-Nano-Machines (BNMs), that extends the existing Internet of Things (IoT) into the nano-scale by leveraging biological mechanisms such as DBMC

The authors acknowledge the financial support by the German Federal Ministry of Research, Technology and Space (BMFTR) in the program of “Souverän. Digital. Vernetzt.”. Joint project 6G-life, project identification number: 16KISK002.

Alexander Wietfeld and Wolfgang Kellerer are with the Chair of Communications Networks at Technical University of Munich, 80333 Munich, Germany (e-mail: alexander.wietfeld@tum.de, wolfgang.kellerer@tum.de).

Parts of this paper were presented at the IEEE ICC 2024 [1] and discussed in a short letter to T-MBMC [2], see Section I-B.

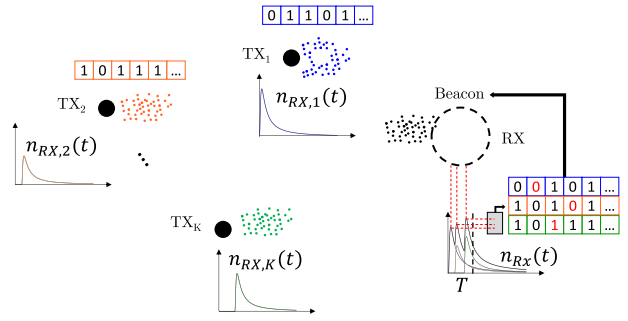


Fig. 1: Schematic representation of the DBMC-aNOMAly protocol, including NOMA transmission from many TXs to a single RX, the pilot-symbol-based parameter optimization scheme, as well as the beacon sent out by the RX to avoid worst-case offset scenarios.

for specific applications. Predicted use cases range from the agricultural sector and laboratory settings, to future medical approaches. For example, ongoing research is exploring the ideas of infection and tumor detection [5], cardiovascular system monitoring [6], or targeted drug delivery [7]. It is important to consider that BNMs will largely be synthetic cells or tiny nano-robots with severely limited resources and capabilities. On the other hand, a large number of BNMs will be deployed at once. In order to realize the complex use cases described above, it is essential to create DBMC networks for communication and collaboration between different BNMs [1], [8]. Additionally, systems within the IoBNT lack the general computing capabilities that are the foundation of traditional electromagnetic (EM)-based networks. Therefore, we will need specifically adapted and simplified computing approaches so that individual BNMs can follow algorithm steps, make decisions and optimize parameters [2], [9], [10].

The first step towards a comprehensive DBMC networked system is an efficient multiple access (MA) scheme. For example, MA could ensure that a receiver (RX) BNM can differentiate the content and sources of messages arriving from multiple transmitter (TX) BNMs. In this paper, we present and evaluate a novel non-orthogonal multiple access (NOMA) scheme for DBMC networks that provides benefits over classical orthogonal MA schemes like time-division multiple access (TDMA) (higher throughput) and molecule-division multiple

access (MDMA) (single-molecule-type), as shown in [1]. Then, we propose a simple and effective protocol for parameter optimization and operation of the scheme. A simple schematic representation is shown in Figure 1. In the following, we will thoroughly analyze the related work on MA schemes for DBMC, parameter optimization methods and protocols, identify remaining gaps, and outline the novel contributions of this work. This paper is a comprehensive extension of our previous work on NOMA for DBMC networks [1] and error probability optimization for MA [2].

A. Related Work

A number of MA schemes have been proposed and analyzed for DBMC networks. Each is based on utilizing a physical resource to be distributed to users. For the purposes of this paper, we will view the schemes from the perspective of a network with a single RX and multiple TXs.

TDMA utilizes the time dimension, sequentially assigning a time slot to each TX, in which it can transmit a message [11], [12]. To implement TDMA, all TXs need to be tightly synchronized with each other and they can all use the same molecule type for transmission.

The MDMA scheme assigns a different molecule type to each TX, making it possible for the RX to differentiate the messages into separate streams, even if they arrive simultaneously [13], [14], increasing the capacity of the network. However, growing numbers of different molecules are necessary for larger networks and the physical complexity of the RX grows, as more receptor types are required. Jamali et al. have explored an extension of MDMA by allowing for mixtures of molecule types similar to the olfactory system [15].

The use of the amplitude dimension for MA in DBMC was first proposed in [16], where the number of received molecules from each TX is defined as a source address and a set of amplitudes is designed such that the sum of a certain subset is unique to a certain set of active TXs. Applying a constant bit error probability (BEP), the authors utilize a maximum likelihood decoder based on a deterministic codebook of received amplitudes. The system lacks the capability to adapt to random or changing conditions and the assumptions of the underlying physical scenario are not tailored to real DBMC networks.

NOMA has received significant attention in the context of classical EM communication in recent years [17], due to its capability to increase the network capacity without requiring more frequency channels. Power-domain NOMA, its most common form, is based on different levels of received signal power at the RX. If we compare EM communication and DBMC, there are analogies between frequency channels and molecule types, as well as signal power, and the received number of molecules. The motivation to employ NOMA in DBMC networks, therefore, comes from the idea of increasing the DBMC network capacity with simultaneous transmission from all TXs, while utilizing only a single molecule type, limiting the physical complexity of the RX.

The adapted NOMA for DBMC networks (DBMC-NOMA) scheme from [1] has been shown to match the performance

of MDMA, as long as communication parameters including detection thresholds and the emitted number of molecules are chosen optimally. However, the previous work only considered the case where all TXs are synchronized with each other, simplifying the mathematical analysis, but leading to severe performance limitations. Similar to discussions for traditional NOMA [18], and as we will show in this paper, extending the analytical model to the asynchronous case between all TXs can yield significant performance improvements by reducing the multiple-access interference (MAI). Additionally, the work in [1] did not address the question of implementation hurdles for NOMA, particularly, the optimal choice of parameters in a practical system and the increased complexity due to the successive interference cancellation (SIC) mechanism.

There are different approaches for finding the optimal parameters in a DBMC system, usually to minimize the BEP or similar metrics. To start with, it is possible to sample the analytical expression with sufficient resolution to determine the optimum parameters via exhaustive search, as performed in [1] for the DBMC-NOMA system. For sufficiently high resolution and if the search domain is chosen appropriately, this will yield the global optimum. However, the effort is extremely high and it is not feasible in a practical system or for growing network size.

Secondly, we can consider finding an analytical solution to the BEP minimization. For example, Chouhan et al. [19] derive closed-form expressions for the optimal number of transmitted molecules and detection thresholds for a single-link (as opposed to an MA-based) DBMC system. This approach requires the expression to be analytically tractable, which becomes less likely for more complex networks. Additionally, the evaluation of complex analytical expressions will not be feasible in real-time under changing conditions, considering the limited capability of the TXs and RXs, as well as the necessary amount of accurate information as input to the expression.

Global optimization algorithms represent another option, as Cheng et al. [20] have demonstrated by applying gradient-descent and particle swarm optimization to optimize the decision thresholds in a two-way single-link DBMC system. These algorithms usually require only that the BEP expression can be evaluated. Again however, this requirement will be hard to fulfill by individual DBMC nodes given the necessary operations and information to achieve this.

Data-driven or machine learning methods are often utilized when little information is available about the system model. For example, Qian et al. [21] implement a neural network capable of choosing the optimal detection thresholds in a single-link DBMC system. The implementation of neural networks within biological systems based on chemical reactions and diffusion is a topic of ongoing research [10] and simple neural networks could be implemented even in low-capability DBMC systems. However, the neural network used in works like [21] are not designed with biological implementation in mind, while the networks in [10] are not shown to perform complex tasks such as optimization. Overall, the general nature of data-driven approaches might make them inefficient for the resource-constrained environments found in DBMC networks, and more targeted methods could also fulfill the task.

Lastly, specific heuristic algorithms have been proposed, largely based on pilot symbol transmission and very simple logical and mathematical operations. The motivation for these approaches stems from the fact that simple operations such as comparisons or additions have been shown to work as chemical reaction networks (CRNs), i.e. can be computed with chemical inputs and outputs [22]. Heinlein et al. [9] have demonstrated the first fully chemical simulation model of a molecular RX including a simple pilot-symbol-based algorithm. In our previous work, we have proposed a first version of an optimization heuristic for the DBMC-NOMA scheme [2] and have simulated a version based on CRNs [23]. However, the system in [2] is limited to only 2 TXs and explores only few variable parameters, assumes perfect global synchronization, and relies on a complex feedback channel for the optimization of the emitted number of molecules, all of which we will address in this paper.

B. Contributions and extension of previous work

In this work, we build upon our previous work [1], [2] to make the following novel contributions:

- 1) We present a comprehensive analytical model for an asynchronous NOMA system for DBMC networks with K TXs, one RX, incorporating L symbols of inter-symbol interference (ISI).
- 2) We derive the analytical BEP expression of this system assuming a diffusion-based Poisson channel and verify the result using Monte Carlo simulations (MCSs).
- 3) Using the analytical results, we present a comparison between TDMA, MDMA and DBMC-NOMA focusing specifically on different scenarios of synchronization offset. We show that effectively utilizing the offset can significantly improve the performance of DBMC-NOMA, outperforming TDMA and matching MDMA in much harsher conditions compared to the synchronized DBMC-NOMA scheme considered in [1] and [2], as long as certain worst-case scenarios are avoided.
- 4) Furthermore, we propose a pilot-symbol-based optimization protocol for asynchronous DBMC-NOMA (DBMC-aNOMA), capable of adaptively choosing detection thresholds, optionally adapting the number of transmitted molecules, and including a worst-case-offset avoidance mechanism (WCAM). Adapted to the asynchronous system by considering the individual offsets, the protocol represents a significant extension of the version considered in [2] and is designed using simple CRN-compatible operations.
- 5) Lastly, DBMC-aNOMA is thoroughly analyzed with regard to its BEP reduction capabilities under various conditions using MCSs. We show that DBMC-aNOMA works under different levels of noise, ISI, and sampling jitter, changing channel conditions, and its performance benefits increase for larger networks with $K > 2$. Additionally, results indicate that the WCAM renders the high-effort optimization step for the number of emitted molecules at the TX side unnecessary in most cases, decreasing the protocol complexity significantly.

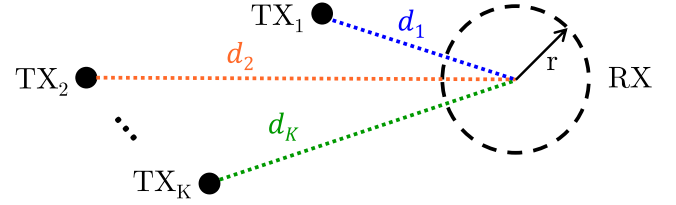


Fig. 2: DBMC scenario with K point TXs at distances $d_1, d_2 \dots d_K$ from a spherical RX.

The remainder of this paper is structured as follows:

In Section II, the channel model and communication system assumptions are introduced, as well as the asynchronous system model for TDMA, MDMA, and DBMC-NOMA. Section III contains the analytical derivation of the BEP for the considered system. Based on this derivation, in Section IV, we conduct a thorough evaluation of the different MA schemes. Using the insights gained, we propose and explain the DBMC-aNOMA protocol in Section V and present the results of extensive MCSs in Section VI. Lastly, we conclude the paper with Section VII.

An overview of all acronyms used throughout the paper can be found in the following table.

LIST OF ACRONYMS	
Acronym	Full term
BEP	bit error probability
BNM	Bio-Nano-Machine
CRN	chemical reaction network
DBMC	diffusion-based molecular communication
DBMC-aNOMA	asynchronous NOMA with pilot-symbol optimization protocol for DBMC
DBMC-NOMA	NOMA for DBMC networks
EM	electromagnetic
IoBNT	Internet of Bio-Nano-Things
IoT	Internet of Things
ISI	inter-symbol interference
MA	multiple access
MAI	multiple-access interference
MCS	Monte Carlo simulation
MDMA	molecule-division multiple access
MI	mutual information
NOMA	non-orthogonal multiple access
OOK	on-off-keying
RX	receiver
SIC	successive interference cancellation
SNR	signaling-molecule-to-noise ratio
TDMA	time-division multiple access
TX	transmitter
UCA	uniform concentration assumption
WCAM	worst-case-offset avoidance mechanism

II. SCENARIO AND SYSTEM MODEL

This section will introduce the physical scenario and define a simple channel model. Additionally, the communication system is described in detail, including the basic principle of the considered MA schemes.

A. Channel Model

Figure 2 depicts the basic communication scenario considered in the following. The network consists of a single RX and

K TXs at distances d_1, d_2, \dots, d_K , where TX_i is at distance d_i from the RX. The RX is assumed to be a passive spherical observer with radius r , representing a common simple RX model [24]. The TXs are modeled as point sources which are capable of emitting instantaneous pulses of molecules. This represents a good approximation compared to a volume TX as long as the channel is sufficiently long [24]. The surrounding channel is assumed to be unbounded free space. Accordingly, free diffusion affects the emitted molecules with diffusion coefficient D . Firstly, we will focus on the single-link channel between a TX_i and the RX. If TX_i releases a single molecule at $t = 0$, we can solve the diffusion equation to find the probability of observing this molecule within the RX volume $V_{\text{RX}} = \frac{4}{3}\pi r^3$ at time t as [24]

$$P_i(t) = P(t, d_i) = \frac{V_{\text{RX}}}{(4\pi D t)^{\frac{3}{2}}} \exp\left(-\frac{d_i^2}{4Dt}\right). \quad (1)$$

For (1), we apply the uniform concentration assumption (UCA) inside the RX, which is approximately valid for sufficiently long channels compared to the RX size, i.e. $r < 0.15 \cdot d_i$ [24]. Now, we consider that TX_i releases $N_{\text{TX},i}$ molecules simultaneously and $N_{\text{TX},i}$ is sufficiently large compared to the received number of molecules $n_{\text{RX},i}(t)$. Additionally, as is typical [24], the propagation of individual molecules is assumed independent. Then, $n_{\text{RX},i}(t)$ can be modeled as a Poisson distributed random variable $n_{\text{RX},i}(t) \sim \mathcal{P}(\lambda_i(t))$ with mean and variance equal to

$$\lambda_i(t) = N_{\text{TX},i} P_i(t). \quad (2)$$

B. Communication System

For the modulation scheme, we utilize on-off-keying (OOK), i.e. $N_{\text{TX},i}$ molecules are released for a bit-1 and nothing for a bit-0. Time is split into slots of length T . The current time slot, starting at $t = 0$ and ending at $t = T$ is denoted as slot $l = 0$, while the preceding L slots are denoted as $l \in \{1, 2, \dots, L\}$. The symbol sent by each TX_i in time slot l is $s_i[l] \in \{0, 1\}$ with 0 and 1 equally likely. Every TX emits a pulse of $s_i[l] N_{\text{TX},i}$ molecules at time $t_{\text{off},i}$ within the current time slot, where $0 \leq t_{\text{off},i} < T$. Therefore, as opposed to previous work in [1], [2], we do not generally assume synchronization between the TXs, which could be excessively complicated, particularly as the number of TXs K increases. Also, in contrast to [1], we do not need accurate channel knowledge and distance information at the RX. However, we require that the RX acquires an estimated sampling time for each TX. This could be possible in practice by having multiple oscillating CRNs within the RX that react to a certain pulse trigger sent by each TX or from an external source, described similarly in [9], [25]. We will not model this process explicitly, but the uncertainty of the sampling time is incorporated in the following. We denote all the RX-side processes associated with a certain TX by the index j to differentiate it from the sending side. We model the acquisition process of the sampling time $t_{\text{s},j}$ for the symbol from TX_j by imposing a uniform distribution around the actual peak time $t_{\text{p},j} = \frac{d_j^2}{6D} + t_{\text{off},j}$. This results in

$$t_{\text{s},j} \sim \mathcal{U}(t_{\text{p},j} - \Delta_{\text{p}}/2, t_{\text{p},j} + \Delta_{\text{p}}/2) \quad (3)$$

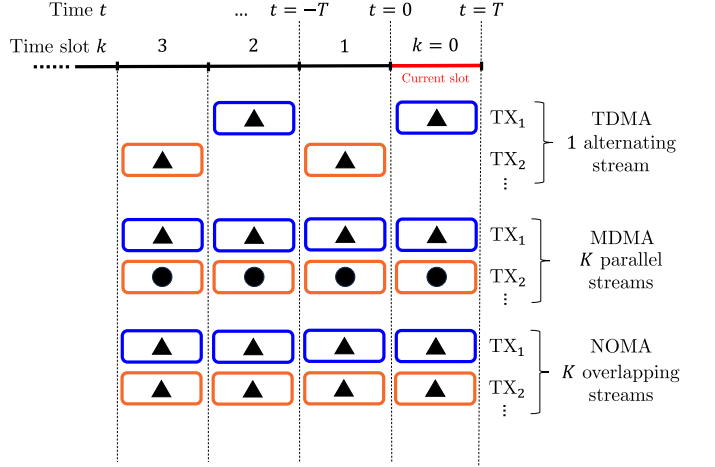


Fig. 3: Comparison of resource allocation for different MA schemes. The triangle and circle shape signify different molecule types, the color is associated with different TXs, and the horizontal placement in the time slots shows the allocation of transmissions over time.

with the sampling jitter Δ_{p} . Then, the average signal component sent by TX_i for a transmitted bit-1 and sampled at the sampling time of TX_j in time slot l is

$$\lambda_{i,j}[l] = \lambda_i(t_{\text{s},j} + lT). \quad (4)$$

Additionally, we denote the *desired average sample*, i.e. the average contribution at $t_{\text{s},i}$ for a bit-1 from TX_i in the current time slot as

$$\tilde{\lambda}_i = \lambda_{i,i}[0] = \lambda_i(t_{\text{s},i}). \quad (5)$$

The total signal at the RX for a certain sampling point, $n_{\text{RX}}(t_{\text{s},j})$, is a sum of multiple independent Poisson random variables $n_{\text{RX},i}(t_{\text{s},j})$ with means either equal to 0 or according to (2). Therefore, the sum is also a Poisson random variable with its mean the sum of the means of the added random variables. Additionally, we assume an additive Poisson noise component with mean λ_n . The calculation of the sum depends on the offsets $t_{\text{off},i}$ and the utilized MA scheme and will be detailed in the following section.

C. Multiple Access Schemes

We will consider three separate MA schemes for the analytical evaluation, namely MDMA, TDMA, and DBMC-NOMA. The calculation of the average received signal for the Poisson distribution will be derived for each scheme in the following. An overview of the resource allocation using time and molecule type is shown in Figure 3 for illustrative purposes.

a) Molecule-Division Multiple Access (MDMA): Starting with MDMA, each TX utilizes one of K different molecule types. We assume that they are perfectly distinguishable at the RX such that K parallel channels are created, which we can analyze separately. It is assumed that each TX transmits a symbol in every time slot l and that all molecule types share the diffusion coefficient D . We can consider the signal

received from any TX_j without loss of generality, and it can be expressed as

$$n_{\text{RX},j}^{\text{MDMA}}(t_{s,j}) \sim \mathcal{P} \left(\lambda_n + s_j[0]\tilde{\lambda}_j + \sum_{l=1}^L s_j[l]\lambda_{j,j}[l] \right) \quad (6)$$

ISI

We can see that this contains the *desired sample* component $s_j[0]\tilde{\lambda}_j$ as well as ISI. Then, the sample taken by the RX to detect the symbol sent by TX_j in the current time slot is $n_{s,j}^{\text{MDMA}} = n_{\text{RX},j}^{\text{MDMA}}(t_{s,j})$. Threshold detection is applied according to

$$\hat{s}_j = \begin{cases} 1 & n_{s,j}^{\text{MDMA}} \geq \tau_j^{\text{MDMA}} \\ 0 & n_{s,j}^{\text{MDMA}} < \tau_j^{\text{MDMA}}, \end{cases} \quad (7)$$

with the detected symbol \hat{s}_j and the set of thresholds $\mathcal{T}^{\text{MDMA}} = \{\tau_j^{\text{MDMA}}\}_{j=1}^K$.

b) *Time-Division Multiple Access (TDMA)*: In TDMA, we assume all TXs use the same molecule type and they are assigned different time slots in sequential order. When the current time slot is assigned to TX_j , then each previous time slot $l > 0$ was assigned to $\text{TX}_{[(j-l-1) \bmod K]+1}$, i.e. continuing in descending order and looping around to TX_K at $l = j$. Then, the received signal is the sum of all signals emitted by the TXs and, sampled at $t_{s,j}$, is given by

$$n_{\text{RX}}^{\text{TDMA}}(t_{s,j}) \sim \mathcal{P} \left(\lambda_n + s_j[0]\tilde{\lambda}_j \cdots \right. \\ \left. + \sum_{l=1}^L s_{[(j-l-1) \bmod K]+1}[l]\lambda_{[(j-l-1) \bmod K]+1,j}[l] \right) \quad (8)$$

ISI

It includes ISI from previous time slots, in which various other TXs were transmitting. To detect the symbol transmitted by TX_j , assigned to the current time slot, we use the sample $n_{s,j}^{\text{TDMA}} = n_{\text{RX}}^{\text{TDMA}}(t_{s,j})$ and apply detection

$$\hat{s}_j = \begin{cases} 1 & n_{s,j}^{\text{TDMA}} \geq \tau_j^{\text{TDMA}} \\ 0 & n_{s,j}^{\text{TDMA}} < \tau_j^{\text{TDMA}}, \end{cases} \quad (9)$$

with the set of detection thresholds $\mathcal{T}^{\text{TDMA}} = \{\tau_j^{\text{TDMA}}\}_{j=1}^K$.

c) *Non-Orthogonal Multiple Access for DBMC Networks (DBMC-NOMA)*: In the following, we utilize and extend the initial definition of DBMC-NOMA from our previous work [1], [2]. All TXs transmit in each time slot using the same molecule type, as shown in Figure 3. The received signal at the sampling time $t_{s,j}$ for TX_j will include contributions from past transmission, i.e. ISI, as well as from other TXs in the same time slot, i.e. MAI. The resulting formula is given by

$$n_{\text{RX}}^{\text{NOMA}}(t_{s,j}) \\ \sim \mathcal{P} \left(\lambda_n + s_j[0]\tilde{\lambda}_j + \underbrace{\sum_{\substack{i=1 \\ i \neq j}}^K s_i[0]\lambda_{i,j}[0]}_{\text{MAI}} + \underbrace{\sum_{i=1}^K \sum_{l=1}^L s_i[l]\lambda_{i,j}[l]}_{\text{ISI}} \right). \quad (10)$$

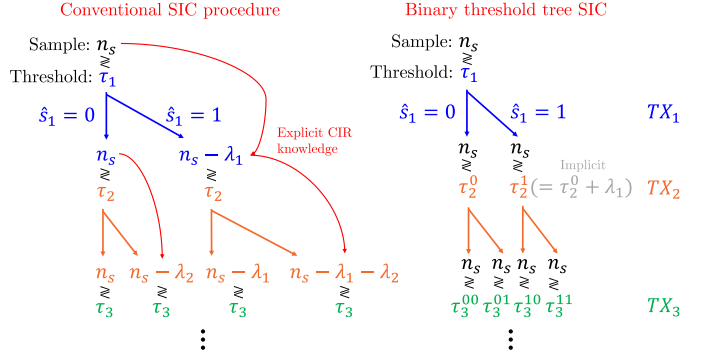


Fig. 4: Successive interference cancellation (SIC) implementation strategies: the diagram on the left shows the classical description of a SIC procedure, in which knowledge of the individual channel impulse response (CIR) is used to subtract the respective contribution from TX_i , λ_i , from the sampled signal n_s . On the right, the equivalent threshold-adaptation-based version is shown, which uses a set of thresholds $\tau_i^{\hat{s}_{i-1}}$ for every TX resulting in a binary-tree-like structure, in which the same sample is compared many times.

To reduce the impact of the additional MAI, SIC is used by the RX. Detection is performed sequentially from TX_1 to TX_K , i.e. within the current time slot, multiple detection events take place, one for each TX.

Usually, for classical power-domain NOMA in EM networks, the contribution of the currently considered TX is removed from the received signal sample after detection using channel estimation information about the average expected signal contribution. This process of detection is depicted on the left side of Figure 4. As proposed and described in our previous work [2], SIC together with single-sample threshold detection can also be described as a multi-stage binary tree threshold detection procedure using the sample $n_{\text{sample},j}^{\text{NOMA}} = n_{\text{RX}}^{\text{NOMA}}(t_{s,j})$. For detecting the symbol sent by TX_j , the decision rule becomes

$$\hat{s}_j = \begin{cases} 1 & n_{\text{sample},j}^{\text{NOMA}} \geq \tau_j^{\hat{s}_{j-1}} \\ 0 & n_{\text{sample},j}^{\text{NOMA}} < \tau_j^{\hat{s}_{j-1}}. \end{cases} \quad (11)$$

Here, the vector of detected symbols $\hat{s}_{j-1} = [\hat{s}_1, \dots, \hat{s}_{j-1}]$ helps to form the set of thresholds $\mathcal{T}_j^{\text{NOMA}} = \{\tau_j^{0\dots00}, \tau_j^{0\dots01}, \tau_j^{0\dots10}, \dots, \tau_j^{1\dots11}\}$ with 2^{j-1} thresholds used for TX_j . As highlighted in Figure 4, this approach is equivalent to the traditional approach, if we implicitly assume that the thresholds are calculated according to the rule described above. However, the binary tree threshold procedure provides significantly more flexibility for optimization and does not explicitly necessitate channel knowledge to set up.

III. ANALYTICAL BIT ERROR PROBABILITY DERIVATION

We denote the BEP of the individual TX_i as $P_{e,i}$. Additionally, we consider the system BEP $P_{e,\text{sys}}$ as the probability that any transmitted symbol in a given time slot is erroneously detected:

$$P_{e,\text{sys}} = \frac{1}{K} \sum_{i=1}^K P_{e,i}. \quad (12)$$

In the following, we present the derivation of $P_{e,\text{sys}}$ for a network of K TXs according to Figure 2. We begin with DBMC-NOMA and later also address TDMA and MDMA. To keep the derivation tractable, the sampling jitter Δ_p is disregarded for the analytical evaluation.

For preparation, we introduce auxiliary variables based on the definitions from Section II. Firstly, we write the vector of all average sampling values taken at $t_{p,j}$, for transmission from all TXs in all time slots as

$$\Lambda_j = [\lambda_{1,j}[0], \dots, \lambda_{K,j}[0], \lambda_{1,j}[1], \dots, \lambda_{K,j}[1], \dots, \lambda_{1,j}[L], \dots, \lambda_{K,j}[L]]. \quad (13)$$

Secondly, we define the set of all vectors of length N with binary elements as $\mathbb{B}^N = \{[b_0 b_1 b_2 \dots b_N] \mid b_i \in \{0, 1\}\}$. Based on this, we write the vector of the transmitted symbols by all TXs in all time slots as

$$\mathbf{S} = [s_1[0], \dots, s_K[0], s_1[1], \dots, s_K[1], \dots, s_1[L], \dots, s_K[L]] \in \mathbb{B}^{K(L+1)}, \quad (14)$$

such that

$$\begin{aligned} \mathbf{S} \cdot \Lambda_j &= \sum_{i=1}^K \sum_{l=0}^L s_i[l] \lambda_{i,j}[l] \\ &= \underbrace{\sum_{\substack{i=1 \\ i \neq j}}^K s_i[0] \lambda_{i,j}[0]}_{\text{MAI}} + \underbrace{\sum_{i=1}^K \sum_{l=1}^L s_i[l] \lambda_{i,j}[l]}_{\text{ISI}}, \end{aligned} \quad (15)$$

as in (10). Similarly, we reuse the vector of all the decoded symbols in the current time slot for the TXs up to and including TX_m, previously defined for the SIC thresholds in Section II

$$\hat{\mathbf{s}}_m = [\hat{s}_1, \hat{s}_2, \dots, \hat{s}_m] \in \mathbb{B}^m. \quad (16)$$

We will now consider the case of decoding the symbol from TX_j in the current time slot after having decoded the symbols of TX₁ to TX_{j-1}. We define the probability of the sample for TX_j after SIC being below the threshold $\tau_j^{\hat{s}_{j-1}}$ given that TX_j transmitted symbol $s_j[0] = x \in \{0, 1\}$ as

$$P_{j,x} = \mathbb{P}(n_{\text{sample},j}^{\text{NOMA}} < \tau_j^{\hat{s}_{j-1}} \mid s_j[0] = x). \quad (17)$$

Using $\mathcal{P}_{\text{CDF}}(m; \lambda) = \sum_{k=0}^m \lambda^k \frac{e^{-\lambda}}{k!}$, which denotes the evaluation of the cumulative density function of the Poisson distribution at m , we can calculate the conditional probability associated with $P_{j,x}$ when all transmitted symbols \mathbf{S} and the previously decoded symbols $\hat{\mathbf{s}}_{j-1}$ are given, as

$$\begin{aligned} \mathbb{P}(n_{\text{sample},j} < \tau_j^{\hat{s}_{j-1}} \mid s_j[0] = x, \mathbf{S} = \mathbf{S}', \hat{\mathbf{s}}_{j-1} = \hat{\mathbf{s}}'_{j-1}) \\ &= \mathcal{P}_{\text{CDF}}\left(\tau_j^{\hat{s}_{j-1}} - 1; \mathbf{S}' \cdot \Lambda_j + \lambda_n\right). \end{aligned} \quad (18)$$

To arrive at the marginal probability, we must form the sum over all possible cases for \mathbf{S} (with $s_j[0] = x$) and $\hat{\mathbf{s}}_{j-1}$ multiplied by the respective probability of occurrence for each case. Since there are symbols across $L+1$ time slots from K different TXs considered in the received signal, there are $2^{K(L+1)}$

different equiprobable combinations of transmitted symbols \mathbf{S} , which affect the mean of the received signal's Poisson distribution. Additionally, 2^{j-1} different possible combinations of detected symbols $\hat{\mathbf{s}}_j$ for the previously considered TXs in the current time slot affect the choice of $\tau_j^{\hat{s}_{j-1}}$ for the SIC procedure. The probability of each \hat{s}_j occurring depends on \mathbf{S} and on the BEPs for the previously considered TXs. We note that therefore, $\mathbb{P}(\mathbf{S} = \mathbf{S}' \in \mathbb{B}^{K(L+1)} \mid s_j[0] = x) = \frac{1}{2^{(K(L+1)-1)}}$.

To calculate the probability of occurrence of the previous $j-1$ decoded symbols, $\hat{\mathbf{s}}_{j-1}$, we first note that it can be written as the following multiplication of conditional probabilities of a single decoded symbol

$$\begin{aligned} \mathbb{P}(\hat{s}_{j-1} = \hat{s}'_{j-1} \mid \mathbf{S} = \mathbf{S}', s_j[0] = x) \\ = \prod_{i=1}^{j-1} \mathbb{P}(\hat{s}_i = \hat{s}'_i \mid \mathbf{S} = \mathbf{S}', s_j[0] = x, \hat{\mathbf{s}}_{i-1} = \hat{\mathbf{s}}'_{i-1}). \end{aligned} \quad (19)$$

To now calculate the individual factors, we first define

$$\begin{aligned} P_{\text{prev}}(j, \mathbf{S}, \hat{\mathbf{s}}_{j-1}) &= \\ \mathcal{P}_{\text{CDF}}\left(\tau_j^{\hat{s}_{j-1}} - 1; \mathbf{S} \cdot \Lambda_j + \lambda_n\right). \end{aligned} \quad (20)$$

The probability of a decoded symbol is then expressed for the four different possible cases as follows

$$\begin{aligned} \mathbb{P}(\hat{s}_j = \hat{s}'_j \mid \mathbf{S} = \mathbf{S}', s_j[0] = x, \hat{\mathbf{s}}_{j-1} = \hat{\mathbf{s}}'_{j-1}) \\ = \begin{cases} 1 - P_{\text{prev}}(j, \mathbf{S}, \hat{\mathbf{s}}_{j-1}) & s_{j,0} = \hat{s}_j \text{ AND } s_{j,0} = 0 \\ 1 - P_{\text{prev}}(j, \mathbf{S}, \hat{\mathbf{s}}_{j-1}) & s_{j,0} \neq \hat{s}_j \text{ AND } s_{j,0} = 1 \\ P_{\text{prev}}(j, \mathbf{S}, \hat{\mathbf{s}}_{j-1}) & s_{j,0} = \hat{s}_j \text{ AND } s_{j,0} = 1 \\ P_{\text{prev}}(j, \mathbf{S}, \hat{\mathbf{s}}_{j-1}) & s_{j,0} \neq \hat{s}_j \text{ AND } s_{j,0} = 0 \end{cases}. \end{aligned} \quad (21)$$

Inserting (20) into (21), and (21) into (19) yields the result for $\mathbb{P}(\hat{s}_{j-1} = \hat{s}'_{j-1} \mid \mathbf{S} = \mathbf{S}', s_j[0] = x)$. Combining (19) with (17) and (18), we get

$$\begin{aligned} P_{j,x} &= \sum_{\mathbf{S}' \in \mathbb{B}^{K(L+1)}} \sum_{\substack{\hat{\mathbf{s}}'_{j-1} \in \mathbb{B}^{j-1} \\ s_j[0]=x}} \mathbb{P}(\hat{s}_{j-1} = \hat{s}'_{j-1} \mid \mathbf{S} = \mathbf{S}', s_j[0] = x) \\ &\quad \cdot \frac{1}{2^{(K(L+1)-1)}} \mathcal{P}_{\text{CDF}}\left(\tau_j - 1; \mathbf{S}' \cdot \Lambda_j + \lambda_n\right). \end{aligned} \quad (22)$$

We note that $P_{j,x}$ corresponds to the probability of correct detection if $x = 0$, and to the probability of incorrect detection if $x = 1$. Therefore, the BEP of TX_j is given by

$$P_{e,j} = \frac{1}{2} (P_{j,1} + (1 - P_{j,0})). \quad (23)$$

Similar but simpler derivations exist for TDMA [12], and MDMA, for which we consider K independent communication links [26].

IV. ANALYTICAL EVALUATION

In the following, we will utilize the analytical model to evaluate the properties of DBMC-NOMA under various conditions and analyze the importance of different parameters on the performance. Subsequently, we will conduct a comprehensive comparison of DBMC-NOMA with TDMA and MDMA.

A. Performance Metrics

To measure the system's performance, we will utilize two metrics depending on the evaluated scenario and context.

- 1) The system BEP, $P_{e,sys}$, as described in Section III will be used to evaluate the performance between different scenarios that use the same MA scheme. Specifically, we will use it to investigate the effects of parameters on the performance of DBMC-NOMA.
- 2) The mutual information (MI) [27] can be derived from the probability distributions of transmitted and received symbols and represents the amount of bits of information that can be conveyed from TX to RX. MI due to a transmission from TX_i in the current time slot is denoted as \mathcal{I}_i . For MDMA and NOMA all TXs transmit in all time slots. In contrast, the MI for TDMA must be averaged across the K TXs since one TX transmits at a time. Therefore, we will utilize MI particularly for the comparison between the different MA schemes.

Additionally, the signaling-molecule-to-noise ratio (SNR) is utilized as a measure of relative noise level and is defined as the ratio between the expected signal $\tilde{\lambda}_i$ and the additive noise for each TX_i

$$\text{SNR} = 20 \log_{10} \frac{\tilde{\lambda}_i}{\lambda_{n,i}}. \quad (24)$$

B. Monte-Carlo Simulations

To validate the analytically derived results with another method, MCSs were conducted for matching scenarios. Here, the Poisson distributions of the received signals were sampled for a large number of randomly generated symbol vectors and the different MA schemes were applied. The number of generated symbols varies according to the analytical results, as we need many more samples to accurately estimate an error rate of 10^{-6} compared to 10^{-3} .

C. Parameter Analysis for DBMC-NOMA

In the following, results are focused on specific aspects of DBMC-NOMA to highlight isolated effects of different parameters on the performance.

1) *Optimizing the Detection Threshold:* In Figure 5, $P_{e,i}$ is plotted over the respective τ_1 and τ_2^0 for a system with $K = 2$ TXs. For ease of demonstration in the plot, it is assumed that $\tau_1^1 = \tau_2^0 + \tilde{\lambda}_1$, mirroring the classical SIC scheme in Figure 4. The number of transmitted molecules is chosen as $N_{\text{TX},1} = 10^6$ and $N_{\text{TX},2} \approx 0.5 \cdot 10^6$. All other parameters correspond to the default values in Table I. The optimization process of the thresholds for DBMC-NOMA can be conducted iteratively, similar to the structure of the SIC procedure. The optimum threshold τ_1^* can be chosen independently of the thresholds for TX₂. Then, the choice of τ_2^0 and τ_1^1 depends on the resulting $P_{e,1}^*$. In Figure 5, $P_{e,2}$ is shown for $\tau_1 = \tau_1^*$ and therefore, a fixed $P_{e,1}$. Subsequently, we can choose τ_2^{0*} at the minimum of the orange line plot. The figure shows clearly how we can identify a unique optimum value for the detection thresholds in the DBMC-NOMA system. This procedure could be continued similarly for network sizes $K > 2$ using the same principle,

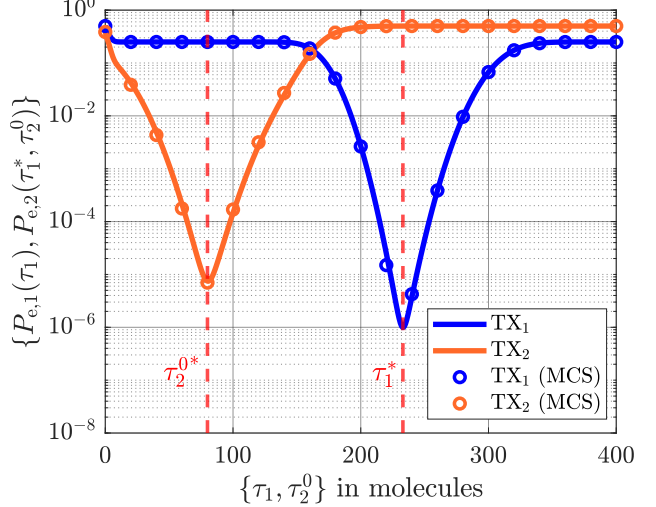


Fig. 5: Analytical BEPs, $P_{e,i}$ over the detection thresholds on the x -axis, for a DBMC-NOMA system with $K = 2$ TXs. MCS results superimposed for validation. We show $P_{e,1}(\tau_1)$, which can be expressed independent of TX₂. Then, for optimal choice τ_1^* , we depict $P_{e,2}(\tau_1^*, \tau_2^0)$. Numbers of emitted molecules are set to $N_{\text{TX},1} = 10^6$, $N_{\text{TX},2} \approx 0.5 \cdot 10^6$. All other parameters according to Table I.

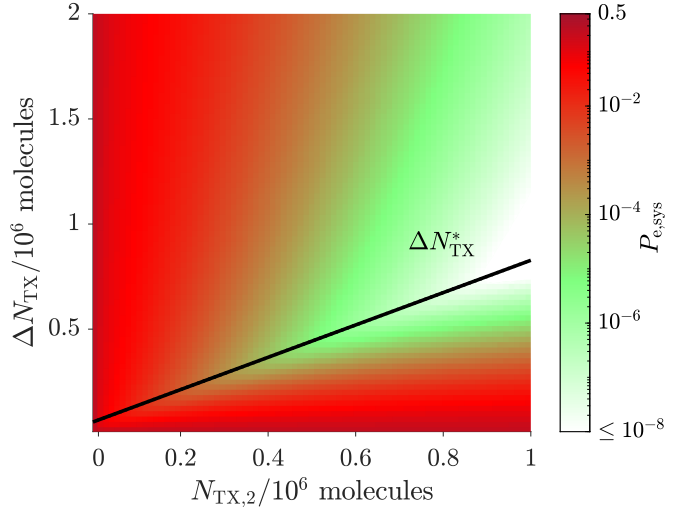


Fig. 6: DBMC-NOMA system BEP $P_{e,sys}$ depicted as a color-coded heatmap with $K = 2$ TXs. Number of emitted molecules of TX₂, $N_{\text{TX},2}$, on the x -axis, and the difference $\Delta N_{\text{TX}} = N_{\text{TX},1} - N_{\text{TX},2}$ on the y -axis. For each point, detection thresholds are chosen optimally. Black line indicates the respective optimum value of ΔN_{TX} w.r.t $P_{e,sys}$ for each value of $N_{\text{TX},2}$. All other parameters according to Table I.

as the thresholds of TX_i are always independent of any TX_j with $j > i$.

2) *Optimizing the Emitted Number of Molecules:* Figure 6 depicts a heatmap of the system BEP $P_{e,sys}$ over a varying $N_{\text{TX},2}$ on the x -axis as well as $\Delta N_{\text{TX}} = N_{\text{TX},1} - N_{\text{TX},2} > 0$ on the y -axis. The network has $K = 2$ TXs. For every point

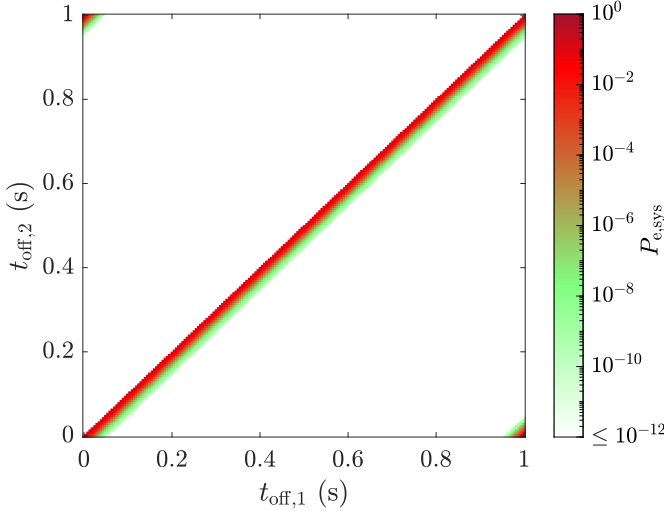


Fig. 7: DBMC-NOMA system BEP, $P_{e,sys}$, depicted as a color-coded heatmap with the synchronization offsets of TX₁, $t_{off,1}$, and TX₂, $t_{off,2}$, on the x - and y -axis, respectively. For all points, the detection threshold were chosen optimally. All other parameters according to Table I.

on the map, the optimum thresholds have been chosen via exhaustive search for the specific combination of $N_{TX,1}$, $N_{TX,2}$. On the graph, we can identify an optimum value ΔN_{TX}^* for each $N_{TX,2}$ forming a line. This is caused by the application of the SIC procedure. If ΔN_{TX} was reduced from the optimum, the separation of signal contributions from each TX would decrease, making it more difficult to choose an appropriate threshold for TX₁, independent of the transmission by TX₂. This is only possible for sufficient difference between the two contributions. $P_{e,1}$ would increase and, therefore, also the detector is more likely to apply the wrong threshold for TX₂, increasing $P_{e,2}$ as well. The standard deviation of the signal in the Poisson model is equal to the square-root of its mean, $\sigma = \sqrt{\lambda}$. As a result, if ΔN_{TX} is increased above the optimum, the signal standard deviation at the RX will increase together with the total signal mean. For TX₁, the relative value $\frac{\sigma}{\lambda} = \frac{1}{\sqrt{\lambda}}$ will actually decrease, since the mean keeps rising with it. However, the signal standard deviation for TX₂ will increase more and more, leading to an increase in $P_{e,2}$.

Following the optimum ΔN_{TX}^* line from left to right, we also observe that lower and lower values of $P_{e,sys}$ are achieved. This is also due to the signal-dependent value of the standard deviation. In this case, however, both $N_{TX,1}$ and $N_{TX,2}$ are increased. Therefore, the standard deviation relative to the mean decreases for both TXs, the detection of both samples is more reliable, and $P_{e,sys}$ decreases.

3) *Varying the Time Offset*: In previous work on DBMC-NOMA [1], [2], only the detection thresholds on the number of emitted molecules were considered as variable parameters in the system to optimize the performance. In this paper, we will also consider the choice of time offset $t_{off,j}$ between different TXs, as defined in Section II. In the previous investigations, the assumption was that the system is fully synchronized and

$t_{off,j} = 0 \forall j$. Relaxing this assumption, Figure 7 depicts a heatmap of $P_{e,sys}$ for a system of 2 TXs and a varying $t_{off,1}$ and $t_{off,2}$ on the x -axis and y -axis, respectively. Same as before, the optimum thresholds were identified via exhaustive search and chosen for each point on the heatmap. Additionally, $N_{TX,1} = N_{TX,2} = 10^6$.

The plot clearly shows very limited areas with a high error probability, which we will denote as *worst-case offset* areas. These correspond to cases with either $t_{off,1} \approx t_{off,2}$ or $t_{off,j} \approx T = 1$. Here, the peaks of the arriving channel impulse responses align, leading to significant MAI, as calculated in Eq. 10 in Section II. Despite the long tail of the DBMC channel impulse response, the peak itself is relatively sharp. Therefore, next to the worst-case offset areas, there is a steep decline in MAI and drop-off in $P_{e,sys}$, even without any optimization of the emitted number of molecules in this case. This suggests that there is a way of optimizing performance by avoiding the worst-case offset areas and simultaneously optimizing the detection thresholds. We will address this later with the worst-case-offset avoidance mechanism (WCAM) in Section V.

D. Comparison of MA Schemes

In this subsection, we will compare the performance of TDMA, MDMA, and DBMC-NOMA under different conditions. The parameters utilized throughout this evaluation are listed in Table I with highlighted default values that are used in the absence of a separate definition. We note, that MDMA acts as an upper-bound target for the performance, as it allows for K entirely independent channels, the performance of which cannot be surpassed by another MA scheme. As described in Section II, the implementation of MDMA would entail a significant increase in system complexity, related to the increased number of different molecule types. Again, the results include the analytical BEP evaluation derived in Section III and MCSs for validation.

1) *Offset Cases*: Four different configurations of DBMC-NOMA will be considered during the evaluation. In all cases, we choose the optimum detection thresholds via exhaustive search.

- *Synchronized (s)*: All TXs send at the same time, i.e. $t_{off,i} = 0 \forall i$. Represents the assumed *worst-case* scenario.
- *Synchronized with optimized number of emitted molecules (s-o)*: $t_{off,i} = 0 \forall i$ and we choose the optimum $N_{TX,i}$ via exhaustive search. This is the same setup used in previous work [1], [2].
- *Random offset (r)*: $t_{off,i}$ are chosen from a random uniform distribution $\mathcal{U}[0, T]$ and the results are averaged over 200 samples. Represents the assumed *average-case* scenario.
- *Even offset (e)*: $t_{off,i}$ are distributed evenly across the range $[0, T]$. Represents the assumed *best-case* scenario.

If $N_{TX,i}$ is optimized, we assume a maximum molecule budget per TX of $N_{TX,max}$, up to which each $N_{TX,i}$ can be varied. For all other cases, we assume $N_{TX,i} = N_{TX,max} \forall i$.

Preliminary results have shown and the mathematical formulas in Section II suggest that TDMA and MDMA are not or

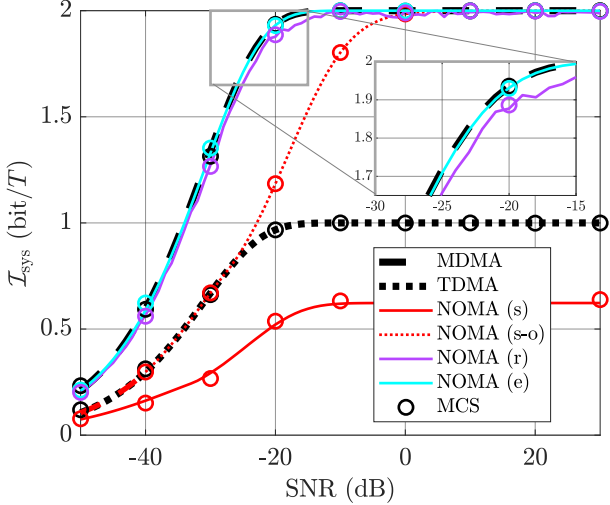
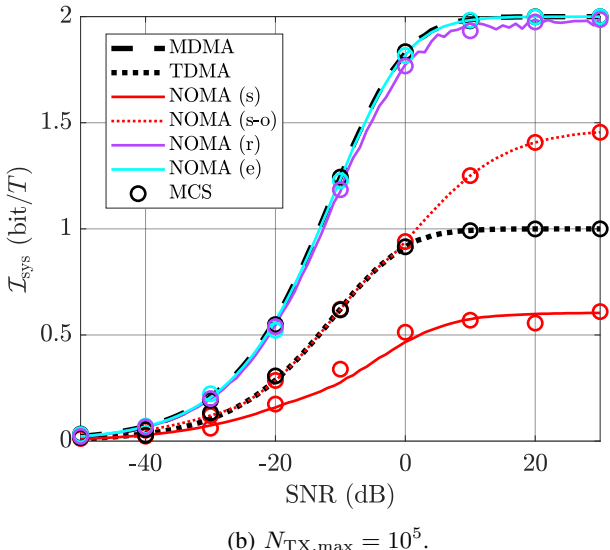
(a) $N_{TX,max} = 10^6$.(b) $N_{TX,max} = 10^5$.

Fig. 8: Mutual information \mathcal{I}_{sys} per symbol period T over the SNR for three different MA schemes, and four different variants of DBMC-NOMA. Synchronized (s), synchronized and N_{TX} optimized ($s-o$), random offsets (r), evenly distributed offsets (e). Analytical results and corresponding MCS are depicted for validation. Detection thresholds are chosen optimally. Results are shown for two different values of the molecule budget per TX, $N_{TX,max}$. For all other parameters see Table I.

only marginally affected by the different offset configurations, due to the lack of MAI. Therefore, we show only one curve for these two schemes.

2) *Varying Noise Level*: Figure 8 shows the mutual information per time slot of the entire system, \mathcal{I}_{sys} , on the y -axis, and the SNR, i.e. the additive noise level, on the x -axis. The results are shown for $K = 2$ and two different values of $N_{TX,max}$. We will start with Figure 8a, where $N_{TX,max} = 10^6$. As expected, MDMA is the upper bound for all schemes. The performance of the different DBMC-NOMA configurations

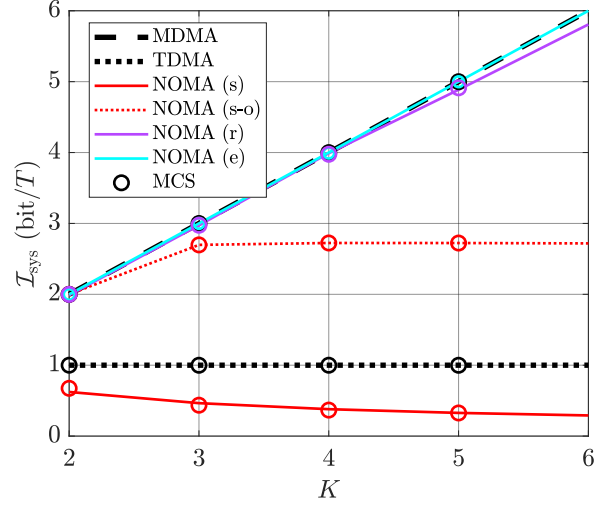


Fig. 9: Mutual information \mathcal{I}_{sys} per symbol period T over the number of TXs, K , for three different MA schemes, and four different variants of DBMC-NOMA. Synchronized (s), synchronized and N_{TX} optimized ($s-o$), random offsets (r), evenly distributed offsets (e). Analytical results and corresponding MCS are depicted for validation. All other parameters according to Table I.

varies significantly. In the (s) case, it performs worse than all schemes including TDMA, due to the significant amount of MAI and the same value of $N_{TX,i}$. For the ($s-o$) case, the MAI is managed more effectively, i.e. $N_{TX,2}$ is reduced as needed. We can observe that $\mathcal{I}_{sys}^{NOMA} \approx \mathcal{I}_{sys}^{TDMA}$ for low SNR, and $\mathcal{I}_{sys}^{NOMA} \approx \mathcal{I}_{sys}^{MDMA} \approx 2 \text{ bit}/T$ for high SNR. However, in both asynchronous cases (r) and (e), DBMC-NOMA always outperforms TDMA and achieves $\mathcal{I}_{sys}^{NOMA} \approx \mathcal{I}_{sys}^{MDMA}$ for all SNR values. The zoomed-in window showcases a slight difference between (r) and (e), where the (r) case always slightly underperforms MDMA and (e). This is due to the unavoidable inclusion of some worst-case offset samples in the averaged result for (r), in which the performance more closely resembles (s).

Looking at Figure 8b, where $N_{TX,max} = 10^5$, we see a similar behavior with slight differences. Firstly, a major disadvantage of the N_{TX} optimization becomes apparent, as the ($s-o$) case does not reach MDMA performance even for very large SNR values. Additionally, the impact of worst-case delay samples in the (r) case appear larger, when comparing the (r) and (e) curve.

3) *Varying Network Size*: The network size K is varied on the x -axis with \mathcal{I}_{sys} on the y -axis in Figure 9. We can observe several crucial effects. Firstly, in the synchronous case (s), the system performance deteriorates with growing number of TXs meaning that existing TXs are negatively affected to a larger extent than the added throughput generated by the new TXs. This is in line with the expected effects of significant MAI. Secondly, the management of N_{TX} in the ($s-o$) case avoids the performance deterioration, but leads to a plateau after a certain network size K is reached. Any added TX_i

TABLE I: Parameters for the Analytical Evaluation

Parameter	Symbol	Values (Default)
Number of TXs	K	2, 3, 4, 5, 6
TX distances	d_i	10 μm
RX radius	r	1 μm
Diffusion coefficient	D	$10^{-9} \text{ m}^2 \text{ s}^{-1}$
Symbol period	T	1 s
ISI symbols	L	{1, 6}
Signaling-molecule-to-noise ratio	SNR	{[-50, 30], ∞ } dB
Molecule budget per TX	$N_{\text{TX},\text{max}}$	[10^5 , 10^6] molecules

will then always be assigned $N_{\text{TX},i} = 0$ after this point, leaving the performance of previous TXs unaffected. Similar to the observations when varying the SNR in Figure 8, DBMC-NOMA in the (e) configuration matches the performance of MDMA for all considered network sizes. In the (r) case, system performance slightly falls short of the upper bound, with the difference growing for higher values of K , as the probability of hitting a worst-case offset sample increases and the performance impact of the (s) case grows simultaneously.

E. Summary of Analytical Evaluation

From the results above we can take away the following main points

- 1) Allowing for the synchronization offset between the TXs as a third variable promises significant performance benefits.
- 2) These performance benefits appear to be larger than the ones provided by the optimization of $N_{\text{TX},i}$, which we will see later involves a large amount of effort.
- 3) It appears that the full potential performance can be achieved, if the few worst-case offset cases can be avoided to close the gap between the (r) and (e) configuration.

V. BEP MINIMIZATION PROTOCOL

We have seen that the detection thresholds, the number of emitted, molecules, and the synchronization offset are the major controllable parameters that influence the performance of a DBMC-NOMA system. Therefore, the following optimization problem can be posed

$$\begin{aligned} \{\mathcal{T}_i^*, t_{\text{off},i}^*, N_{\text{TX},i}^*\}_{i=1}^K &= \arg \min_{\{\mathcal{T}_i, t_{\text{off},i}, N_{\text{TX},i}\}_{i=1}^K} P_{\text{e,sys}} \quad (25) \\ \text{s.t. } N_{\text{TX},i} &\leq N_{\text{TX},\text{max}} \forall i \in 1, \dots, K. \end{aligned}$$

We have derived the calculation of the BEP $P_{\text{e,sys}}$ in Section III. We have previously evaluated and discussed how analytical solutions and global optimization algorithms [19], [20] or data-driven methods will often lead to the optimum values [2]. As discussed in Section I, these approaches are not suited for the requirements in DBMC systems, as they involve significant channel knowledge, accurate evaluations of complex functions and their derivatives, or a large amount of computing power compared to the severely limited capabilities of future nanoscale nodes.

In previous work, we have proposed and evaluated a simple greedy heuristic based on pilot symbols and have shown that

Algorithm 1 Detection Threshold Optimization Algorithm

```

INPUT:  $\mathcal{T}_i^{\text{NOMA}} = \{\tau_i^{\tilde{s}_{i-1}}\} \forall i \in [1, K]$ 
for  $n = 1$  to  $N_{\text{pilot}}$  do
    PILOT SYMBOL:  $\mathbf{s}_n = [s_{n,1}, s_{n,2}, \dots, s_{n,K}]$ 
    for TXs  $i = 1$  to  $K$  do
        TRANSMIT:  $\text{TX}_i \rightarrow s_{n,i} N_{\text{TX},i}$  at  $t_{\text{off},i}$ 
        DETECT: RX uses  $\tau_i^{\tilde{s}_{n,i-1}}$  to obtain  $\hat{s}_{n,i}$ , Eq. 11
        if  $\hat{s}_{n,i} \neq s_{n,i}$  AND  $s_{n,i} = 0$  then
             $\tau_i^{\tilde{s}_{n,i-1}} \leftarrow \tau_i^{\tilde{s}_{n,i-1}} + \Delta\tau$ 
        else if  $\hat{s}_{n,i} \neq s_{n,i}$  AND  $s_{n,i} = 1$  then
             $\tau_i^{\tilde{s}_{n,i-1}} \leftarrow \tau_i^{\tilde{s}_{n,i-1}} - \Delta\tau$ 
    OUTPUT:  $\mathcal{T}_i^{\text{NOMA}} = \{\tau_i^{\tilde{s}_{i-1}}\} \forall i \in [1, K]$ 

```

it reliably attains the optimum values for \mathcal{T}_i and $N_{\text{TX},i}$ [2]. In a different work, we showed how simple operations like comparisons and additions for a DBMC-NOMA scheme can be modeled and simulated as a CRN framework [23]. The optimization heuristic is created using similar operations and could also be modeled as a CRN. Based on those results, we propose an extended pilot-symbol-based protocol, asynchronous NOMA with pilot-symbol optimization protocol for DBMC (DBMC-aNOMA), that improves upon multiple shortcomings of the initial proposal. Firstly, it applies to the asynchronous system defined in Section II removing the need for a high-effort synchronization of the entire network. Secondly, we design a very simple heuristic to avoid the worst-case offset cases, as observed in Section IV, and we will show that we can replace and remove the optimization of the emitted number of molecules. It relied on a complex feedback mechanism between RX and TXs that could be prone to errors [2]. Also, the optimization of the emitted number of molecules can only be defined in a straightforward manner for a system with $K = 2$.

In the following, we will first show the different mechanisms aimed at dealing with detection thresholds \mathcal{T}_i , synchronization offsets $t_{\text{off},i}$, and emitted number of molecules $N_{\text{TX},i}$ separately, and then describe how they are put together to form the DBMC-aNOMA protocol.

A. Optimizing the Detection Thresholds

To heuristically optimize the detection thresholds, we first assume that the other parameters, namely $t_{\text{off},i}$ and $N_{\text{TX},i}$ are fixed for all TX_i . The sequence of pilot symbol vectors known to the RX and all TXs, is denoted as $\mathbf{S}_{\text{pilot}} = [s_{n,i} \in \{0, 1\} \text{ for } 1 \leq n \leq N_{\text{pilot}}, 1 \leq i \leq K]$. The pilot symbol vector of a single pilot iteration is $\mathbf{s}_{\text{pilot},n} = [s_{n,i} \in \{0, 1\} \text{ for } 1 \leq i \leq K]$. The pilot symbol procedure consists of executing the DBMC-NOMA scheme as described in Section II, i.e. all TXs send the bit $s_{n,i}$ for pilot symbol n and the bit from each TX within the symbol period is decoded by the RX in sequence. In addition to the standard procedure, the detection thresholds $\tau_i^{\tilde{s}_{i-1}}$ are adjusted after the transmission, sampling, and decoding of each pilot symbol, starting from an initial value $\tau_{i,\text{init}}^{\tilde{s}_{i-1}} \forall i$. First, the detected symbol for TX_i is compared to the correct symbol in the pilot sequence. If the symbol was detected correctly, the threshold stays the same. If the symbol was incorrectly detected as a

Algorithm 2 Worst-Case-Offset Avoidance Mechanism

```

for  $n = 1$  to  $N_{\text{pilot}}$  do
  PILOT SYMBOL:  $s_n = [s_{n,1}, s_{n,2}, \dots, s_{n,K}]$ 
  for TXs  $i = 1$  to  $K$  do
    TRANSMIT:  $\text{TX}_i \rightarrow s_{n,i} N_{\text{TX},i}$  at  $t_{\text{off},i}$ 
    DETECT: RX uses  $\tau_i^{\tilde{s}_{n,i-1}}$  to obtain  $\hat{s}_{n,i}$ , Eq. 11
     $I_{\text{WCAM}} \leftarrow 0$ 
    if  $\hat{s}_{n,i} \neq s_{n,i}$  then
      if  $s_{n,i} = s_{n,1} \forall_i$  then
         $I_{\text{WCAM}} \leftarrow I_{\text{WCAM}} - 1$ 
      else
         $I_{\text{WCAM}} \leftarrow I_{\text{WCAM}} + \frac{1}{2^{K-1}-1}$ 
    if  $I_{\text{WCAM}} > \tau_{\text{WCAM}} = N_{\text{pilot}}/10$  then
      RX: SEND WCAM BEACON
      OFFSET SEQUENCE:  $\Delta_{s,i} \sim \mathcal{U}[0, \Delta_{s,\text{max}}]$ 
      TX:  $t_{\text{off},i} \leftarrow t_{\text{off},i} + \Delta_{s,i}$ 
  
```

'1', the threshold must be increased, so the detection of a '0' becomes more likely next time. Mirroring this behavior, the threshold is decreased, if the symbol was incorrectly detected as a '0'.

It is important to note that during the pilot symbol process, the thresholds $\tau_i^{\tilde{s}_{n,i-1}}$ are applied for detection, where $\tilde{s}_{n,i-1} = [s_{n,j} \in \{0, 1\} \text{ for } 1 \leq j \leq i-1]$ are the pilot symbols up to and including TX_{i-1} , as opposed to the actually detected symbol vector \hat{s}_{i-1} . This ensures that the thresholds are not optimized for the temporary suboptimal situation at the outset, but with the assumption of correct detection for all previous TXs. The scheme is described in detail in Algorithm 1

B. Avoiding Worst-Case-Offset Scenarios

To start, we assume that $\tau_i^{\tilde{s}_{i-1}}$ and $N_{\text{TX},i}$ remain fixed. To address the choice of synchronization offsets, we note that the results in Section IV have demonstrated that the avoidance of a few narrow worst-case areas for $t_{\text{off},i}$ is enough to achieve upper-bound MDMA performance. Therefore, our approach here is less one of iterative optimization, but of targeted worst-case avoidance. Again, after transmission, sampling and decoding of the pilot symbol, we employ a simple rule to adjust the synchronization offset. The worst-case areas are characterized by the fact that the peaks of multiple TXs roughly align at the RX causing a high level of MAI. The goal is to recognize this using the knowledge available at the RX.

Based on an example system with 2 TXs with overlapping peaks: If both TXs send a '1', the additional MAI is not problematic, since it only pushes the received signal higher, making the detection of a '1' more likely. If both TXs send a '0' it does not matter, since the detection only depends on the noise floor and there is no MAI. However, if the bits sent by the two TXs differ, there is significant MAI that deteriorates the performance of the respective TX that did not send a '1'. Generalizing this observation to network sizes $K > 2$, we have defined rules in Algorithm 2. To identify a likely worst-case-offset scenario, the RX must count the cases where an error occurs for all bits being equal against the cases where all bits are not equal. A significant deviation from the equilibrium indicates a worst-case scenario. When the RX counts past a certain threshold denoted as τ_{WCAM} , it activates the offset

Algorithm 3 Number of Molecules Optimization Algorithm

```

INPUT:  $N_{\text{TX},2}$ 
for  $n = 1$  to  $N_{\text{pilot}}$  do
  PILOT SYMBOL:  $s_n = [s_{n,1}, s_{n,2}, \dots, s_{n,K}]$ 
  for TXs  $i = 1$  to  $K$  do
    TRANSMIT:  $\text{TX}_i \rightarrow s_{n,i} N_{\text{TX},i}$  at  $t_{\text{off},i}$ 
    DETECT: RX uses  $\tau_i^{\tilde{s}_{n,i-1}}$  to obtain  $\hat{s}_{n,i}$ , Eq. 11
    if  $s_{n,2} = 1$  then
      if  $s_{n,1} = 0 \text{ AND } \hat{s}_{n,1} \neq s_{n,1} \text{ AND } \hat{s}_{n,2} = s_{n,2}$  then
         $N_{\text{TX},2} \leftarrow N_{\text{TX},2} \cdot (1 - \alpha_N)$  with probability  $1 - p_{e,f}$ 
      if  $[s_{n,1} = 0 \text{ AND } \hat{s}_{n,1} = s_{n,1} \text{ AND } \hat{s}_{n,2} \neq s_{n,2}]$ 
        OR  $[s_{n,1} = 1 \text{ AND } \hat{s}_{n,1} \neq s_{n,1} \text{ AND } \hat{s}_{n,2} \neq s_{n,2}]$ 
        OR  $[s_{n,1} = 1 \text{ AND } \hat{s}_{n,1} = s_{n,1} \text{ AND } \hat{s}_{n,2} \neq s_{n,2}]$  then
           $N_{\text{TX},2} \leftarrow N_{\text{TX},2} \cdot (1 + \alpha_N)$  with probability  $1 - p_{e,f}$ 
  
```

beacon, sending a pulse of molecules using a separate type of control channel molecules. There is no further information or complex bit sequence contained in the message. Simply, if the TXs recognize the beacon, they apply a predetermined offset to their current sending pattern. The sequence is known to both TXs and RX and can be directly encoded in the pilot sequence $\mathbf{S}_{\text{pilot}}$. The values of additive offset in the offset sequence are uniformly distributed according to $\mathcal{U}[0, \Delta_{s,\text{max}}]$ with the WCAM delay bound $\Delta_{s,\text{max}}$. For $\Delta_{s,\text{max}} = 0$, the WCAM mechanism is deactivated. A detailed pseudo-code version can be found in Algorithm 2.

C. Optimizing the Emitted Number of Molecules

We will now describe the optimization step for the number of emitted molecules $N_{\text{TX},i}$, as proposed in [2], for a system of 2 TXs. We will limit the consideration to this scenario, since any extension will cause a large increase in complexity of the description, and we will show later that the mechanism is not necessary, when using the WCAM above. Similarly to the other two schemes, now, $\tau_i^{\tilde{s}_{i-1}}$ and $t_{\text{off},i}$ remain fixed and the values of $N_{\text{TX},i}$ are adjusted based on the transmission, sampling and decoding of the pilot sequence. It is clear that given the molecule budget $N_{\text{TX},\text{max}}$, one of the TXs should emit exactly the maximum number of molecules, while the other emits a number equal or below. Therefore, for the heuristic, we assume that TX₁ is assigned $N_{\text{TX},1} = N_{\text{TX},\text{max}}$, while $N_{\text{TX},2}$ is optimized via the scheme, starting from an initial value $N_{\text{TX},\text{init}}$. In [2], we showed that this works as long as the distances are sufficiently similar and if the RX can communicate the change in $N_{\text{TX},2}$ to the correct TX, as discussed later in relation to the feedback mechanism. Then, there is a set of decision rules governing the adjustment in $N_{\text{TX},2}$, after determining the detected and correct bits $\hat{s}_{n,1}, \hat{s}_{n,2}$ and $s_{n,1}, s_{n,2}$, respectively.

If $s_{n,2} = 0$, $N_{\text{TX},2}$ does not influence the result and there is no reason for adjustment. For $s_{n,2} = 1$, we will look at two example cases for the adjustment rules. The entire scheme is described in Algorithm 3. If $\hat{s}_{n,1} \neq s_{n,1} = 0$ (incorrectly detected a '1'), and $\hat{s}_{n,2} = s_{n,2} = 1$ (correctly detected a '1'), we can infer that we observed enough molecules at the RX to correctly detect a '1' for TX₂, but the MAI for TX₁ seems to have caused too many molecules to arrive, so that we misclassified its symbol. Therefore, $N_{\text{TX},2}$ should be reduced.

If $\hat{s}_{n,1} = s_{n,1} = 0$ (correctly detected a '0'), and $\hat{s}_{n,2} \neq s_{n,2} = 1$ (incorrectly detected a '0'), we can infer that the MAI for the TX_1 detection was not too high, but the received molecules for TX_2 were not high enough to cross the threshold for a '1'. Therefore, $N_{\text{TX},2}$ should be increased.

1) *Feedback Mechanism Model*: To incorporate the effects of a feedback channel, we propose a simple model. Assuming the RX communicates the necessary adjustment back to TX_2 via a separate control channel molecule and encodes the information using orthogonal binary sequences decoded via correlation, a binary erasure channel appears as an appropriate simplification. Due to the lack of interference from the main communication molecule channel, the information is either recovered correctly, or erased entirely, when the correlation is unsuccessful. To adjust $N_{\text{TX},2}$, a multiplicative model is used, such that

$$N_{\text{TX},2} \leftarrow \begin{cases} N_{\text{TX},2} & \text{with prob. } p_{e,f} \\ N_{\text{TX},2} \cdot (1 \pm \alpha_N) & \text{else,} \end{cases} \quad (26)$$

with the *number of molecules multiplier* α_N . If not otherwise specified, $p_{e,f} = 0$.

D. DBMC-aNOMAl Protocol

In Algorithms 1, 2, and 3, we have respectively assumed that the other parameters stay fixed. Therefore, we propose a joint optimization scheme by alternatingly applying the three algorithms, thereby, focusing on one parameter at a time, but optimizing the entire system across multiple iterations. We define a number of joint algorithm iterations N_{iter} . In each iteration, the algorithm for each parameter, $\tau_i^{\hat{s}_{i-1}}$, $t_{\text{off},i}$, and $N_{\text{TX},i}$ is executed once with N_{pilot} pilot symbols. Due to the focus on the threshold optimization and the WCAM, the default assumption is that Algorithms 1 and 2 are applied, while the execution of Algorithm 3 is optional and will not be applied unless otherwise mentioned.

VI. PROTOCOL EVALUATION

In this section, we will conduct an in-depth evaluation of the DBMC-aNOMAl protocol using MCSs based on randomly generated pilot sequences and the application of the Poisson channel model as introduced in Section II including an evaluation of the effects of sampling jitter as defined in Subsection II-B. We will investigate a number of different scenarios by varying the network size K , the noise level, the considered ISI, the sampling jitter, the inclusion of Algorithm 3, as well as changing parameters during runtime to emulate more realistic situations. For each result, the full protocol run has been repeated at least 100 times, while for particularly high-variance scenarios, i.e. for low SNR or large sampling jitter, we utilized up to 1000 repetitions. We will start with an exemplary analysis of the effects of the WCAM, looking at the interventions and the change in synchronization offset it causes. Then, extensive results for the systematic parameter analysis will be presented. An overview of the simulation parameters can be found in Table II. The default values, indicated by the underline, are utilized unless otherwise stated.

TABLE II: Parameters for the Protocol Evaluation

Parameter	Symbol	Values (Default)
Communication System		
Number of TXs	K	2, 3, <u>4</u> , 5
TX distances	d_i	{8, <u>10</u> , 12} μm
RX radius	r	1 μm
Diffusion coefficient	D	$10^{-9} \text{ m}^2 \text{ s}^{-1}$
Symbol period	T	1 s
ISI symbols	L	{0, <u>1</u> }
Signaling-molecule-to-noise ratio	SNR	{-10, 0, 10, <u>∞</u> } dB
Sampling jitter	Δ_p	{0, 0.05, 0.1} s
Molecule budget per TX	$N_{\text{TX},\text{max}}$	10^6 molecules
Feedback erasure probability	$p_{e,f}$	{0, 0.5, 0.99}
Protocol Parameters		
WCAM delay bound	$\Delta_{s,\text{max}}$	{0, 0.1, 0.5, <u>1</u> } s
Number of seeds	N_{seed}	{ <u>100</u> , 500, 1000}
Number of pilot symbols	N_{pilot}	100
Number of iterations	N_{iter}	1000
Threshold step	$\Delta\tau$	1 molecule
Number of molecules multiplier	α_N	0.1
Initial thresholds	τ_{init}	[1, 1, 1] molecules
Initial number of molecules	$N_{\text{TX},\text{init}}$	10^6 molecules

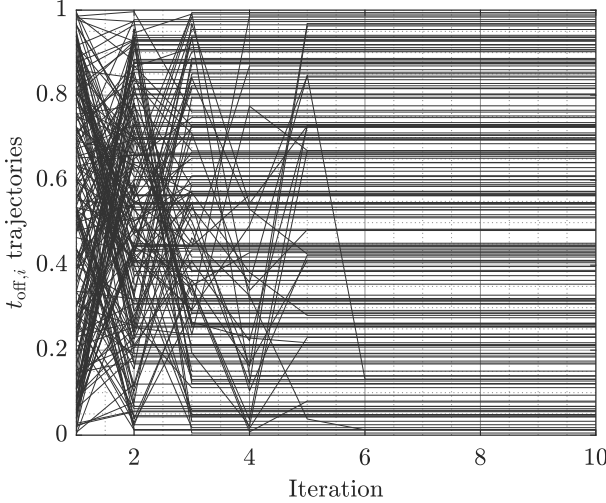
A. Investigating the WCAM

It is relevant, first, to investigate that the WCAM actually has the desired effect of avoiding worst-case offset scenarios. For this, we take one full 100-seed run of DBMC-aNOMAl with default parameters, i.e. 2 TXs, and take a look at the offset statistics. Figure 10a shows the offset values for both TXs, $t_{\text{off},1}, t_{\text{off},2}$ as individual traces over the first 10 iterations for all runs of the protocol. It is important to note that the WCAM beacon is not being sent out in any version of the simulation later than 7 iteration, indicating that there are no recurring offset shifts later in the run. This would indicate a wrong configuration of the protocol and disrupt the optimization procedure severely.

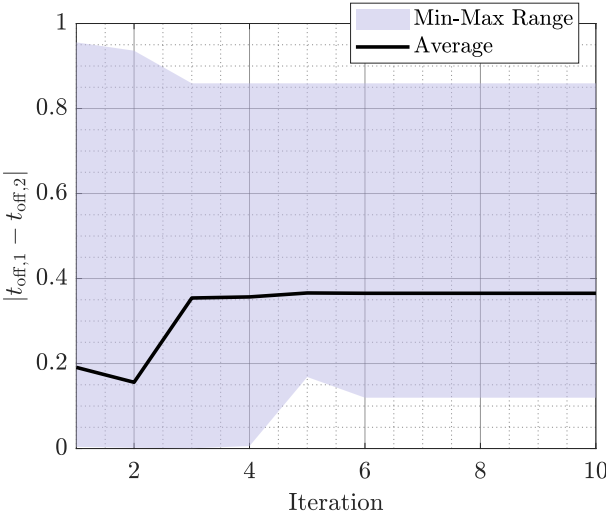
Secondly, Figure 10b shows the average and min-max range of the difference between the two offset values, i.e. $|t_{\text{off},1} - t_{\text{off},2}|$, over all 100 runs and for the first 10 iterations. The plot shows two significant developments. First of all, the range of differences clearly moves away from the two extremes 0 and T , which we had identified as the central points of the worst-case offset areas in Figure 7. Additionally, the mean of the difference stays close and moves towards values of around $0.4T - 0.5T$. Looking back at Figure 7 again, this corresponds to the areas with the best potential BEP performance.

Overall, this example analysis shows that the WCAM can achieve the desired result and avoid the worst-case areas without complex optimization.

In Figure 11, the resulting average BEP trajectories over 1000 iterations are shown for different values of the WCAM delay bound $\Delta_{s,\text{max}}$ between 0 (no WCAM) and T . We can clearly see a significant contrast between the scenarios with and without WCAM, as for $\Delta_{s,\text{max}} = 0$, the large number of badly performing runs cause $P_{e,\text{sys}}$ to approach a constant value very early, while for $\Delta_{s,\text{max}}$, the optimization keeps reducing $P_{e,\text{sys}}$ much further by up to two orders of magnitude. The zoomed-in section highlights the difference between different values of $\Delta_{s,\text{max}}$, i.e. different magnitudes



(a) Plot of all $t_{\text{off},i}$ trajectories for TX₁ and TX₂ superimposed in one plot.



(b) Plot of the mean (black line) and 5%-95% percentile range (shaded area) of the offset difference $|t_{\text{off},1} - t_{\text{off},2}|$.

Fig. 10: Plots for a 100-seed example run of the DBMC-aNOMALy protocol over the first 10 iterations. $K = 2$. All other parameters according to the default in Table II.

of the offset adjustment after the WCAM beacon is sent out. We can observe that the differences are small, however, the performance improves with larger values of $\Delta_{s,\text{max}}$. Therefore, we will choose $\Delta_{s,\text{max}} = T$ as the default going forward.

B. Varying Network Size

In Figure 12, the results with and without WCAM are presented for network sizes between $K = 2$ and $K = 5$. The BEP trajectories illustrate that while $P_{\text{e,sys}}$ expectedly decreases for larger networks, the rate of improvement remains roughly similar and the advantage of DBMC-aNOMALy with the WCAM actually increases slightly, as it is less affected by larger values of K . In general, the protocol deals well

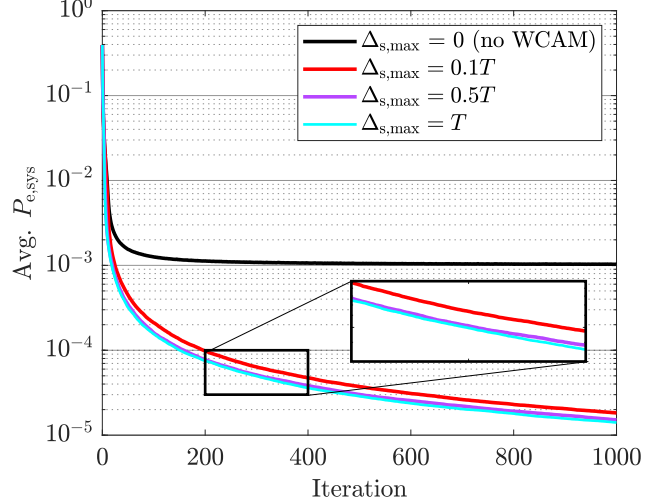


Fig. 11: Average BEP, $P_{\text{e,sys}}$, across 1000 iterations of the DBMC-aNOMALy protocol. Results shown for different values of the WCAM delay bound $\Delta_{s,\text{max}}$, determining the maximum offset induced by the WCAM beacon. $K = 2$. All other parameters according to the default in Table II.

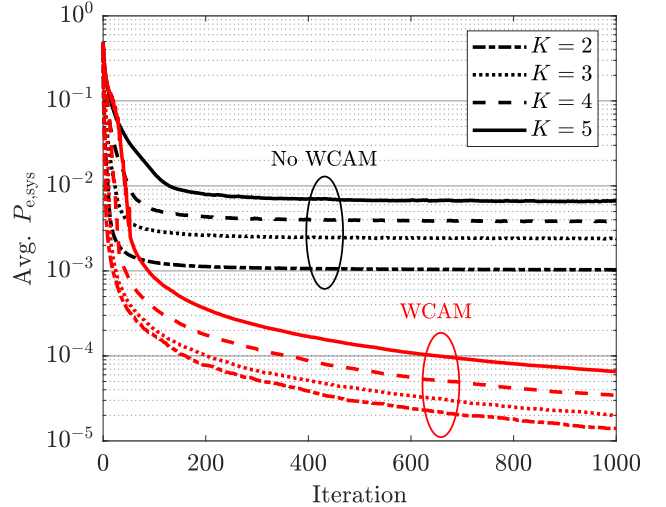


Fig. 12: Average BEP, $P_{\text{e,sys}}$, across 1000 iterations of the DBMC-aNOMALy protocol. Results shown for different values of the number of TXs, K . No WCAM $\rightarrow \Delta_{s,\text{max}} = 0$. WCAM $\rightarrow \Delta_{s,\text{max}} = T$. All other parameters according to the default in Table II.

with increasing K , improving upon previous work, which was limited to networks with $K = 2$ [2].

C. Varying Noise Level

Next, we evaluate the protocols ability to deal with higher levels of noise. Figure 13 showcases average $P_{\text{e,sys}}$ trajectories for DBMC-aNOMALy and SNR values between -10 and 10 dB in addition to the case with no noise (infinite SNR). To avoid cluttering of the figure, we only plot the results without the WCAM for the case of -10 dB. The graph highlights that the

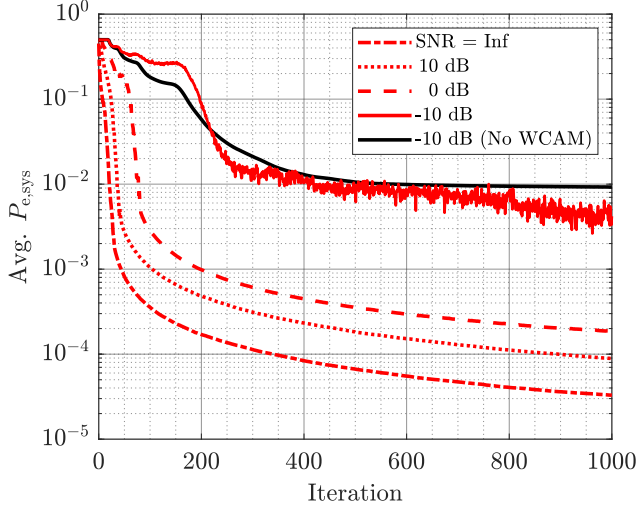


Fig. 13: Average BEP, $P_{e,sys}$, across 1000 iterations of the DBMC-aNOMALy protocol. Results shown for different values of the SNR. No WCAM $\rightarrow \Delta_{s,max} = 0$. WCAM $\rightarrow \Delta_{s,max} = T$. All other parameters according to the default in Table II.

protocol deals handily with the added noise, and the WCAM remains successful for cases down to 0 dB, outperforming the cases without WCAM (not shown explicitly). If the noise gets significant, i.e. SNR = -10 dB, we observe that the performance is similar to the case without WCAM, while still outperforming it slightly. This showcases a potential disadvantage for low SNR environments, where the WCAM becomes more unstable

D. Varying ISI Levels

In Figure 14, the $P_{e,sys}$ trajectory is shown for when ISI is taken into account for 1 past symbol, and when it is not taken into account. Similar to the results in Figure 13, the protocol deals with the ISI well, only dropping slightly in performance in reaction to the added interference.

E. Effect of Sampling Jitter

We have the option to introduce sampling jitter according to the model specified in Section II-B. The results for a system with $K = 2$ TXs is shown in Figure 15. It depicts the average $P_{e,sys}$ trajectory for values of the sampling jitter range Δ_p between 0 and 0.1s.

Comparing the results with and without WCAM, we can observe that the DBMC-aNOMALy protocol is not affected by the sampling jitter and actually achieves the same BEP improvement. However, more variance is introduced as the performance changes more drastically from iteration to iteration since a misaligned sampling point could lead to temporary inaccurate adjustment. Without the WCAM mechanism, sampling jitter leads to a decrease in performance in addition to significant variations.

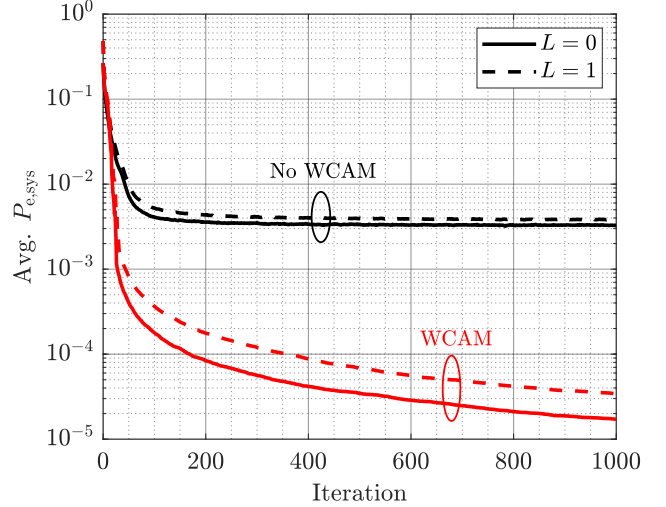


Fig. 14: Average BEP, $P_{e,sys}$, across 1000 iterations of the DBMC-aNOMALy protocol. Results shown for two different values of the number considered ISI symbols, L , in the underlying simulation model. No WCAM $\rightarrow \Delta_{s,max} = 0$. WCAM $\rightarrow \Delta_{s,max} = T$. All other parameters according to the default in Table II.

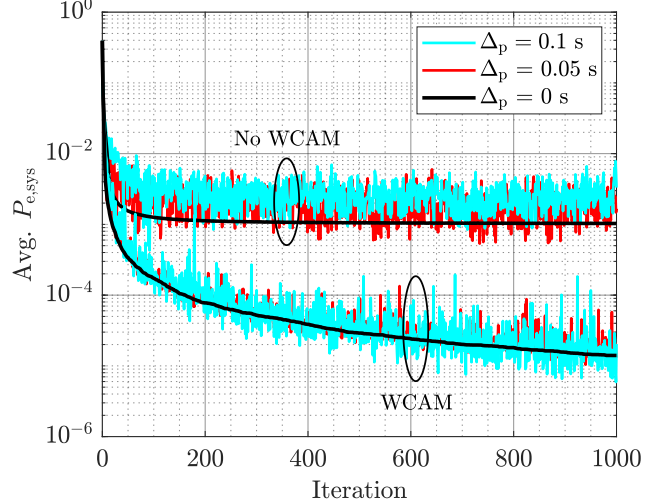


Fig. 15: Average BEP, $P_{e,sys}$, across 1000 iterations of the DBMC-aNOMALy protocol. Results shown for different values of the sampling jitter, Δ_p . No WCAM $\rightarrow \Delta_{s,max} = 0$. WCAM $\rightarrow \Delta_{s,max} = T$. $K = 2$. All other parameters according to the default in Table II.

F. Effect of Optimizing the Number of Emitted Molecules

In Figure 16, we investigate the impact of additional optimization of the number of emitted molecules $N_{TX,i}$, as previously proposed in [2], and defined in Algorithm 3. As discussed in Section V, this version is only defined for $K = 2$ TXs. We show the results for the DBMC-aNOMALy scheme with and without optimizing $N_{TX,i}$, and apply different values for the feedback error probability $p_{e,f}$.

The results show a slight improvement in the performance

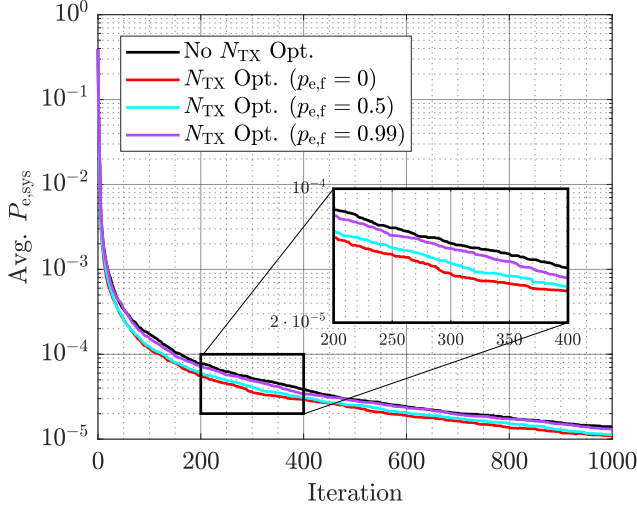


Fig. 16: Average BEP, $P_{e,sys}$, across 1000 iterations of the DBMC-aNOMAl protocol. Results shown with and without the N_{TX} optimization in Algorithm 3 and for different values of the feedback channel error probability $p_{e,f}$. All other parameters according to the default in Table II.

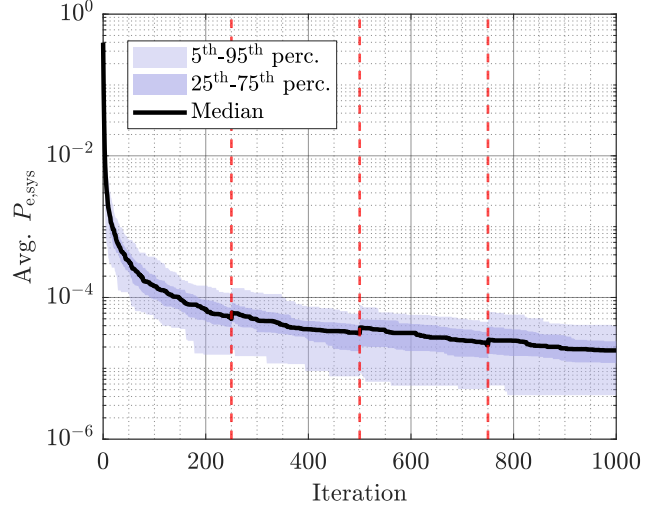
when Algorithm 3 is included, and the impact of up to $p_{e,f} = 0.5$ is very small. For a very unreliable feedback channel ($p_{e,f} = 0.99$), performance deteriorates back to the scenario without Algorithm 3. Overall, the improvement in $P_{e,sys}$ is relatively minor, especially, compared to the improvement between the algorithm with and without WCAM, as shown in Figure 11. The $N_{TX,i}$ feedback mechanism introduces a significant amount of complexity. Therefore, we conclude that in the considered scenario, the performance benefits do not justify the added complexity and effort compared to the standard version of DBMC-aNOMAl including Algorithm 1 and 2.

G. Varying Parameters during Runtime

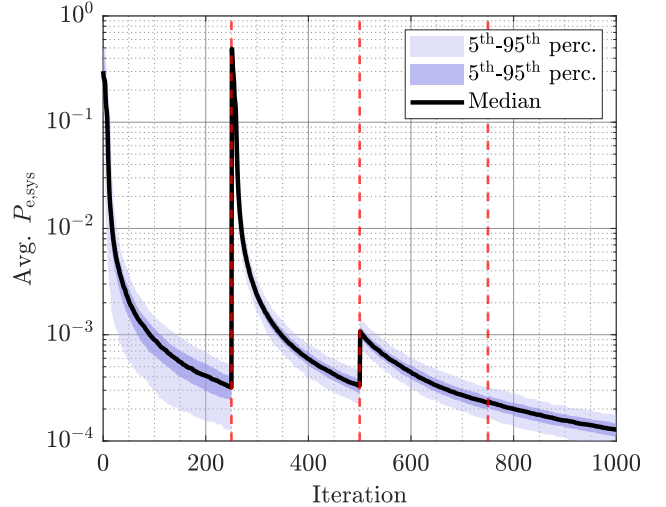
Lastly, we aim to demonstrate the robustness of the DBMC-aNOMAl protocol against fluctuations during the runtime, as would be observed in real moving and changing systems. In Figure 17, we consider two cases: Firstly, Figure 17a, where the distance of TX_1 is varied intermittently, as if it was moving. And secondly, Figure 17b, where the SNR changes at multiple points, emulating varying channel conditions and the appearance of different sources of noise.

Starting with Figure 17a, the distance d_1 of TX_1 from the RX is adjusted from $8\text{ }\mu\text{m}$ to $12\text{ }\mu\text{m}$ in 3 steps at equidistant points across the 1000 iterations. The graph shows the median, as well as two different percentile ranges to also show the possible impact on the distribution. The figure shows that the changes in distance leave little impact on the $P_{e,sys}$ trajectory as well as percentile ranges, indicating the optimization procedure can deal with it without issues.

For Figure 17b, the SNR was varied between 0 and 100 dB via three step-wise adjustments across 1000 iterations. In this case, we see a significant effect on the $P_{e,sys}$ trajectory for the



(a) Distance d_1 varied from $8\text{ }\mu\text{m}$ to $12\text{ }\mu\text{m}$.



(b) SNR varied from 0 to 100 dB.

Fig. 17: Average BEP, $P_{e,sys}$ (black line), and 25%-75% and 5%-95% percentile ranges (inner and outer shaded area, respectively), across 1000 iterations of the DBMC-aNOMAl protocol. Results shown for variation of either distance or SNR in three steps. The time of the change is indicated by the vertical red dashed lines. $K = 2$. All other parameters according to the default in Table II.

first two steps. For example, in the first step, the SNR changes from 0 to approx. 33 dB, which represents a significant shift in the received number of molecules, due to the reduction in noise. Therefore, the current detection thresholds will be off by quite a margin. We can observe that the DBMC-aNOMAl protocol is able to decrease the error to the levels before the change before the next change occurs. Especially, we see a quick error reduction in the first couple of iterations after the initial change. The last step from 66 to 100 dB represents only a small change in absolute noise level, to which the algorithm can adapt almost without visible disruption. The percentile ranges in all cases show that the abrupt change does not cause

an increase in the variability of the optimization outcome, but rather that almost all trajectories follow a very similar path.

VII. CONCLUSION AND FURTHER WORK

In this paper, we have presented an asynchronous system model based on NOMA for DBMC networks with K TXs and one RX, addressing the basic outline of possible future IoBNT networking scenarios. The analytical BEP of the system was derived and thoroughly evaluated for varying network size, noise level, and communication parameters. We identified the detection thresholds, the emitted number of molecules, and the synchronization offsets as the main deciding factors for the performance. Then, we showed that in comparison to existing schemes like TDMA and MDMA, the DBMC-NOMA scheme can match the upper-bound MDMA performance, under almost all conditions, if the detection thresholds are optimized, and certain worst-case configurations of synchronization offset are avoided. Subsequently, we proposed and comprehensively evaluated a novel optimization protocol for DBMC-NOMA systems based on pilot symbols, DBMC-aNOMAly. Using three separate simple algorithms designed to be implementable using chemical reaction networks, the protocol iteratively optimizes the most crucial communication parameters while avoiding the worst-case offset configurations to reduce the BEP of the system. The results show significant robustness of the algorithm under different channel conditions, for different network sizes, as well as subject to sampling jitter. Lastly, we showed how the DBMC-aNOMAly protocol could work in real time under changing conditions.

We aim to address explicit modeling of the protocol as a chemical reaction network in future work, as well as the initial network setup and sampling procedure. Additionally, the DBMC-NOMA scheme should be evaluated experimentally to validate analytical and simulation-based results.

REFERENCES

- [1] A. Wietfeld, S. Schmidt, and W. Kellerer, "DBMC-NOMA: Evaluating NOMA for Diffusion-Based Molecular Communication Networks," in *Proc. IEEE ICC*, Jun. 2024.
- [2] ——, "Error Probability Optimization for Non-Orthogonal Multiple Access in DBMC Networks," *IEEE Trans. Mol. Biol. Multi-Scale Commun.*, vol. 10, no. 3, Sep. 2024.
- [3] N. Farsad, H. B. Yilmaz, A. Eckford, C.-B. Chae, and W. Guo, "A Comprehensive Survey of Recent Advancements in Molecular Communication," *IEEE Commun. Surv. Tutor.*, vol. 18, no. 3, 2016.
- [4] I. F. Akyildiz, M. Pierobon, S. Balasubramaniam, and Y. Koucheryavy, "The Internet of Bio-Nano Things," *IEEE Commun. Mag.*, vol. 53, no. 3, Mar. 2015.
- [5] J. T. Gómez, A. Kuestner, K. Pitke, J. Simonjan, B. D. Unluturk, and F. Dressler, "A Machine Learning Approach for Abnormality Detection in Blood Vessels via Mobile Nanosensors," in *Proc. ACM SenSys '21*. ACM, Nov. 2021.
- [6] P. Hofmann, S. Schmidt, A. Wietfeld, P. Zhou, J. Fuchtmann, F. H. P. Fitzek, and W. Kellerer, "A Molecular Communication Perspective on Detecting Arterial Plaque Formation," *IEEE Trans. Mol. Biol. Multi-Scale Commun.*, vol. 10, no. 3, Sep. 2024.
- [7] U. A. K. Chude-Onkonwo, R. Malekian, B. T. Maharaj, and A. V. Vasilakos, "Molecular Communication and Nanonetwork for Targeted Drug Delivery: A Survey," *IEEE Commun. Surv. Tutor.*, vol. 19, no. 4, 2017.
- [8] A. Bienau, H. Boche, C. Deppe, F. H. P. Fitzek, P. Hofmann, W. Kellerer, W. Labidi, A. Richter, F. C. Simmel, and A. Wietfeld, "Molecular Communication for 6G Networks," in *6G-life: Unveiling the Future of Technological Sovereignty, Sustainability and Trustworthiness*. Academic Press, 2025.
- [9] B. Heinlein, L. Brand, M. Egan, M. Schäfer, R. Schober, and S. Lotter, "Closing the Implementation Gap in MC: Fully Chemical Synchronization and Detection for Cellular Receivers," *IEEE Trans. Mol. Biol. Multi-Scale Commun.*, vol. 11, no. 1, Mar. 2025.
- [10] S. Angerbauer, W. Haselmayer, F. Enzenhofer, T. Pankratz, R. Khanzadeh, and A. Springer, "Molecular Nano Neural Networks (M3N): In-Body Intelligence for the IoBNT," in *Proc. IEEE ICC*, Jun. 2024.
- [11] E. Shitiri and H.-S. Cho, "A TDMA-Based Data Gathering Protocol for Molecular Communication via Diffusion-Based Nano-Sensor Networks," *IEEE Sensors J.*, vol. 21, no. 17, Sep. 2021.
- [12] H. K. Rudarsi, N. Mokari, M. R. Javan, E. A. Jorswieck, and M. Orooji, "Drug Release Management for Dynamic TDMA-Based Molecular Communication," *IEEE Trans. Mol. Biol. Multi-Scale Commun.*, vol. 5, no. 3, Dec. 2019.
- [13] L. Chouhan and M.-S. Alouini, "Rescaled Brownian Motion of Molecules and Devices in Three-Dimensional Multiuser Mobile Molecular Communication Systems," *IEEE Trans. Wirel. Commun.*, vol. 21, no. 12, Dec. 2022.
- [14] X. Chen, M. Wen, C.-B. Chae, L.-L. Yang, F. Ji, and K. K. Igorevich, "Resource Allocation for Multiuser Molecular Communication Systems Oriented to the Internet of Medical Things," *IEEE Internet Things J.*, vol. 8, no. 21, Nov. 2021.
- [15] V. Jamali, H. M. Loos, A. Buettner, R. Schober, and H. Vincent Poor, "Olfaction-inspired MCs: Molecule Mixture Shift Keying and Cross-Reactive Receptor Arrays," *IEEE Trans. Commun.*, vol. 71, no. 4, Apr. 2024.
- [16] B. Krishnaswamy, Y. Jian, C. M. Austin, J. E. Perdomo, S. C. Patel, B. K. Hammer, C. R. Forest, and R. Sivakumar, "ADMA: Amplitude-Division Multiple Access for Bacterial Communication Networks," *IEEE Trans. Mol. Biol. Multi-Scale Commun.*, vol. 3, no. 3, Sep. 2017.
- [17] Y. Saito, Y. Kishiyama, A. Benjebbour, T. Nakamura, A. Li, and K. Higuchi, "Non-Orthogonal Multiple Access (NOMA) for Cellular Future Radio Access," in *2013 IEEE Proc. 77th Veh. Technol. Conf. (VTC Spring)*, Dresden, Germany, Jun. 2013.
- [18] M. Ganji and H. Jafarkhani, "Time Asynchronous NOMA for Downlink Transmission," in *Proc. IEEE WCNC*, Apr. 2019.
- [19] L. Chouhan, P. K. Sharma, and N. Varshney, "Optimal Transmitted Molecules and Decision Threshold for Drift-Induced Diffusive Molecular Channel With Mobile Nanomachines," *IEEE Trans. NanoBiosci.*, vol. 18, no. 4, Oct. 2019.
- [20] Z. Cheng, Y. Tu, K. Chi, and M. Xia, "Optimization of Decision Thresholds in Two-Way Molecular Communication via Diffusion With Network Coding," *IEEE Trans. Mol. Biol. Multi-Scale Commun.*, vol. 8, no. 4, Dec. 2022.
- [21] X. Qian, M. Di Renzo, and A. Eckford, "Molecular Communications: Model-Based and Data-Driven Receiver Design and Optimization," *IEEE Access*, vol. 7, Apr. 2019.
- [22] M. Vasić, D. Soloveichik, and S. Khurshid, "CRN++: Molecular programming language," *Natural Computing*, vol. 19, no. 2, Jun. 2020.
- [23] A. Wietfeld, M. Wendrich, S. Schmidt, and W. Kellerer, "ChemSICAL: Evaluating a Stochastic Chemical Reaction Network for Molecular Multiple Access," in *Proc. IEEE ICC*, Jun. 2025.
- [24] V. Jamali, A. Ahmadzadeh, W. Wicke, A. Noel, and R. Schober, "Channel Modeling for Diffusive Molecular Communication—A Tutorial Review," *Proc. IEEE*, vol. 107, no. 7, Jul. 2019.
- [25] L. F. Borges, M. T. Barros, and M. Nogueira, "A Synchronization Protocol for Multi-User Cell Signaling-Based Molecular Communication," in *Proc. IEEE GLOBECOM*, Dec. 2021.
- [26] L. Shi and L.-L. Yang, "Error Performance Analysis of Diffusive Molecular Communication Systems With On-Off Keying Modulation," *IEEE Trans. Mol. Biol. Multi-Scale Commun.*, vol. 3, no. 4, Dec. 2017.
- [27] T. M. Cover and J. A. Thomas, *Elements of Information Theory*, ser. Wiley Series in Telecommunications. New York: Wiley, 1991.